eng

MDPI

Article

An IoT-Based Technique for Detecting Single-Phase Earth Faults in 6–35 kV Cable Lines Using Current Sensors

Laura Yesmakhanova [1], Zhanat Issabekov [2], Bibigul Issabekova [2,*], Batyrbek Ordabayev [2], Assemgul Zhantlessova [3], Dauren Kudabaev [4] and Olzhas Talipov [2]

1 Faculty of Technology, Department of Automation and Telecommunications, M.Kh. Dulaty Taraz University, 7 Suleimenova St., Taraz 080000, Kazakhstan; laura060780@mail.ru

2 Faculty of Energy, Department of Electrical Engineering and Automation, Toraighyrov University, Building A, Lomov Str. 64, Pavlodar 140008, Kazakhstan; isabekov.g@teachers.tou.edu.kz (Z.I.)

3 Institute of Energy, Department of Electrical Engineering and Automation, S. Seifullin Kazakh Agro Technical Research University, 62 Zhenis, Astana 010008, Kazakhstan; a.zhantlessova@kazatu.edu.kz

4 Relay Protection and Automation Section JSC «KazTransOil», Northern Industrial Zone 263, Pavlodar 140000, Kazakhstan; kutrapali228@mail.ru

* Correspondence: issabekova.b@teachers.tou.edu.kz; Tel.: +7-707-862-3979

Abstract

An IoT-based technique is suggested for detecting single-phase earth faults (SEFs) in 6–35 kV cable networks with an isolated neutral. Unlike existing methods based on measuring zero-sequence currents with traditional current transformers, the suggested technique uses a passive magnetically controlled contact (reed switch) placed in the magnetic field of a cable. This enables recording fault currents of 0.5–2.0 A without external power supply and ensures galvanic isolation. The novelty of this technique is the combination of a reed switch current sensor with an IoT platform: instantaneous values of current are measured by the duration of the closed state of the contacts, then the data are transmitted via a radio channel (LoRa 433 MHz, LoRaWAN, or NB-IoT) to a cloud-based SCADA/EMS system for remote monitoring. The amplitude of the current is calculated from the pickup and resetting currents, as well as the duration of the closed state of the contacts; no high-frequency ADC is required. During experimental tests of a prototype with a KEM-5 reed switch and a TZL-10 current transformer, the difference between the calculated and actual protection operation current was no more than 10–5%. Oscillograms confirmed the correct operation of the device when starting, under load, and during an artificial SEF with a current of 1.6 A. The device response time is a fraction of the industrial frequency period, which significantly reduces the emergency mode duration. The suggested system enables decreasing the system average interruption duration index (SAIDI) and the system average interruption frequency index (SAIFI) by selectively disconnecting a damaged section and preventing cascading faults. The use of two independent channels (current transformer and reed switch) increases the reliability of SEF detection and reduces the risk of false operation. Thus, the developed IoT-based technique improves the reliability, safety, and cost-effectiveness of cable network operation.

Keywords: single-phase earth faults; cable network; IoT; magnetically controlled contact; reed switch; current sensor; relay protection

Check for updates

Academic Editor: Gian Giuseppe Soma

Received: 13 April 2026
Revised: 20 May 2026
Accepted: 22 May 2026
Published: 25 May 2026

1. Introduction

A single-phase earth fault (SEFs) is the most common (up to 80–90%) fault type in 6–35 kV cable networks with an isolated neutral [1–4]. The main difficulties in SEF detection are related to low fault currents (0.5–10 A), instability of arcing processes, and the lack of a direct path for zero-sequence currents. Existing protection methods, such as zero-sequence voltage monitoring, zero-sequence current protection, and power-impressed devices, have a number of limitations: low sensitivity to high-impedance faults [4–6], a need for on-site power supplies, a difficulty of selective disconnection in distributed capacity admittance networks, and a significant time required for fault location by emergency teams [6–8].

Up-to-date approaches to improving the reliability of SEF detection use fiber-optic sensors (DTS/DTSS), partial discharge sensors, and systems based on synchronized phasor measurement units (PMUs). However, these solutions often require expensive equipment, complex calibration, and a developed communications infrastructure, which limits their common use in distribution networks [9,10]. There are low-cost and nonvolatile SEF sensors capable of remotely real-time detecting faults at a level of 0.5–2.0 without the use of traditional saturable current transformers or active electronics in a high-voltage zone.

The novelty of the suggested technique lies in the joint use of (1) a magnetically controlled contact (reed switch) placed in the magnetic field of a cable, which does not require external power supply and directly responds to the field strength proportional to the short-circuit current; (2) a method for determining the amplitude of current by the duration of reed switch closed state without high-frequency sampling; (3) wireless IoT-based data transmission (LoRa, LoRaWAN, NB-IoT) to a cloud platform for centralized monitoring [11–13].

In contrast to known reed switch devices, which were primarily used in position signaling, this work for the first time suggests using them for the quantitative measurement of SEF current and integration with IoT networks [14].

The main tasks of this work were:

- Design of a transformer current sensor with a reed switch;
- Development of a mathematical model which connects the fault current, the reed switch pick-up/resetting currents, and the contact closure time;
- Experimental verification of the model with the use of a physical prototype with a KEM-5 reed switch;
- Development of a data transmission architecture to a SCADA/EMS cloud platform;
- Estimation of SAIDI and SAIFI.

The aim of this work is to develop and experimentally validate an IoT-based technique for detecting SEFs in 6–35 kV cable lines with the use of a highly sensitive and nonvolatile reed switch current sensor, which ensures remote monitoring.

An advantage of using IoT is the possibility of transforming technological processes by means of their quantitative measurability based on the collection and processing of large volumes of data. The integration of IoT technology improves the quality of process and system management by creating conditions for real-time automated decision making and facilitating the optimization of tasks to be solved [1,2].

The scope of IoT encompasses any engineering systems where this technology is used for data exchange. In these systems, IoT devices can function as smart sensors, actuators, gateways for interfacing with industrial networks, etc. Communication protocols enable optimized data transfer through Ethernet networks proving minimal message size and flexible data representation and ensuring data reliability. Implementation of IoT requires organizing the storage and processing of significant volumes of information with the use of databases. Data required for control signal generation can be analyzed both in real time and offline after the information has been saved. This data is then transmitted to actuators.

IoT is focused on managing industrial assets; it ensures continuous online monitoring and operational transparency and increases the efficiency of automation systems. Such devices serve as a basis for assessing personnel productivity, optimizing utilization of production capacities, and monitoring power quality indicators.

https://doi.org/10.3390/eng7060256

Solutions for wireless data communication include LoRaWAN, NB-IoT, and other technologies. In addition, works [15–17] suggested the design of fiber-optic sensors for distributed measurements (DTS/DTSS) mounted along a cable line [18–22]. Partial discharge sensors, which record high-frequency pulses in cable insulation, compose an individual class and are used for early detection of insulation defects which can result in single-phase earth faults (SEF) [23–28]. The aim of this work is the development of an IoT technique for detecting SEFs in 6–35 kV cable networks with the use of current sensors and SEF data transmitting to a control center.

2. Single-Phase Earth-Fault Data Transmission

This work suggests an IoT-based single-phase earth-fault protection system for a 6–35 kV cable network. During our experiments, the protection device operated at SEF currents of approximately 0.5–1.0 A.

Figure 1a shows a block diagram of a setup for picking up signals from a current sensor, with a PC located in close proximity to a measurement point. It is necessary to measure an alternating current in a cable line, which flows through a current transformer, which is an analog current sensor. It does not directly measure the current but records the magnetic field around a conductor through which the current flows. An analog voltage proportional to the current is generated across the sensor output. An Arduino UNO is used as a microcontroller board for measurements, monitoring, and equipment control. The Arduino UNO reads the voltage through an analog input. An internal analog-to-digital converter (ADC) of the Arduino converts analog voltage (0–5 V) into digital. The Arduino microcontroller converts the read values into amperes with the use of a simple sketch (Supplementary Written Program S1). After processing, the data are transmitted to the Ra-02 radio module connected to the Arduino through the SPI interface (MOSI, MISO, SCK, NSS, and other pins). SX1278 modulates signals by LoRa technology (spread spectrum) and transmits them at a frequency of 433 MHz. The second LoRa module connected, for example, to the second Arduino or a computer (Supplementary Receiver and Presentation S1), should be mounted on the receiving side. It receives a radio signal, demodulates it, and transmits data (Supplementary Packages S1) about the current to, e.g., a display, a monitoring system, a server, or a log file [11–14].

Radio signal propagation in underground cable channels.

In urban distribution networks, 6–35 kV cables are laid in trenches, cable channels, and sewers. Direct radio signal propagation from a sensor mounted in a cable chamber or channel to a ground-based LoRaWAN gateway is attenuated due to shielding by reinforced concrete slabs (typically by 10–20 dB) and metal manhole covers (additionally by 5–10 dB). However, experimental studies [12] show that LoRa with SF = 12 and BW = 125 kHz are capable of stably communicating at ranges of up to 300–500 m when a gateway is located 3–5 m above ground. When using a remote sensor antenna at a flexible cable placed inside a cable manhole at a height of 0.5 m from the bottom, the loss for penetration through the reinforced concrete slab does not exceed 15 dB, which ensures reliable reception. For deep collectors (more than 5 m) or long tunnels, it is recommended to install LoRa repeaters spaced 200–300 m apart or use NB-IoT technology (if a provider supports coverage in underground structures). Therefore, the suggested architecture is feasible in typical urban cable channels under conditions of correct selection of gateway points and antenna types.

Architecture of the IoT-based system for SEF detection

The suggested protection system implements decentralized detection logic with centralized coordination. It is based on three principles:

- Hardware independence: the reed switch sensor requires no external power and passively operates.

- Local preprocessing: primary filtering and calculation of the amplitude of current are performed by a field microcontroller (Arduino).
- Cloud coordination: the final decision about the presence of a SEF and its selective clearing is made on the SCADA/EMS platform taking into account data from all network sensors (Table 1).

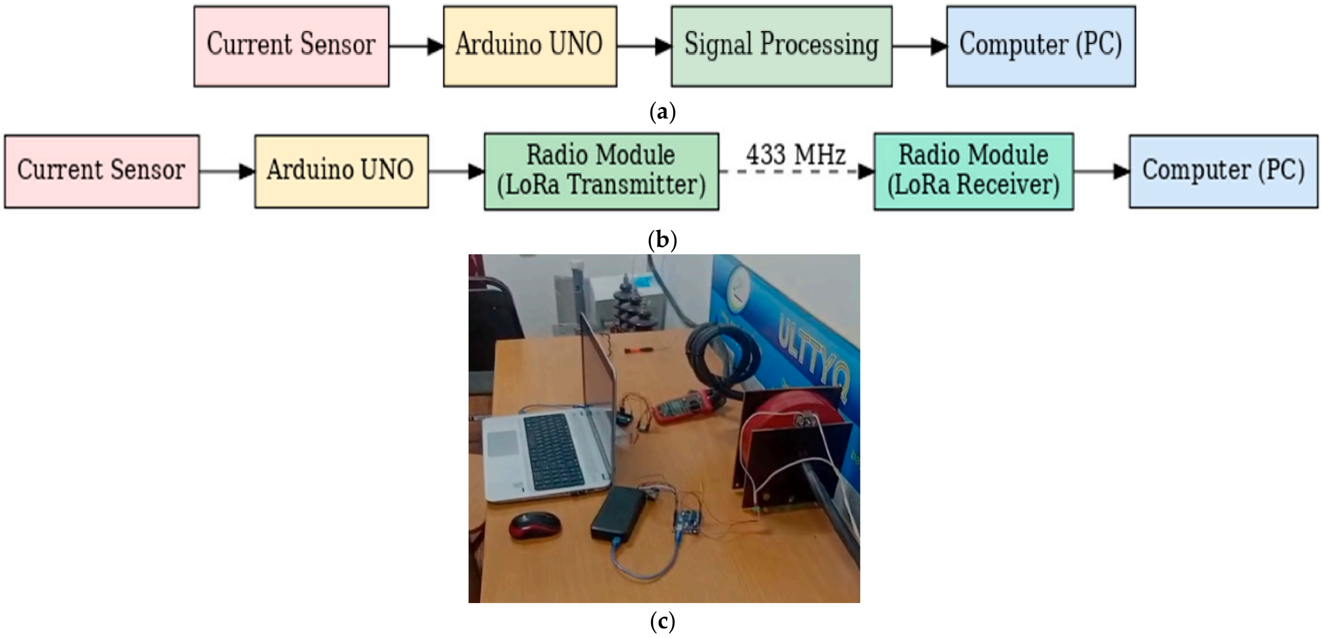

Figure 1. Diagram of signal release from a transformer current sensor: (**a**) pick up current sensor signal circuit; (**b**) IoT data transmission; (**c**) experimental setup.

Table 1. Decision algorithm (steps).

Step	Operation	Responsible Component	Time, ms
1	Measurement of the duration of the closed state of reed switch contacts t1	Timer (Arduino)	0.1–10 (depends on current)
2	Local filtering (median, 5 samples)	Arduino	1
3	Calculation of the amplitude I_m	Arduino	<1
4	Packet assembly (I_m, t01, time tag)	Arduino	<1
5	LoRa → gateway → cloud transmission	LoRa + 4G	50–300
6	Aggregation of data from all network sensors	Cloud SCADA	100
7	Comparison with settings and selective decision	Cloud SCADA	50
8	Triggering (in the case of event)	SCADA → driver	100

The total time from SEF occurrence to triggering is 250–500 ms (depending on the channel load).

System architecture (levels).

The system has a three-layer architecture (Figure 2).

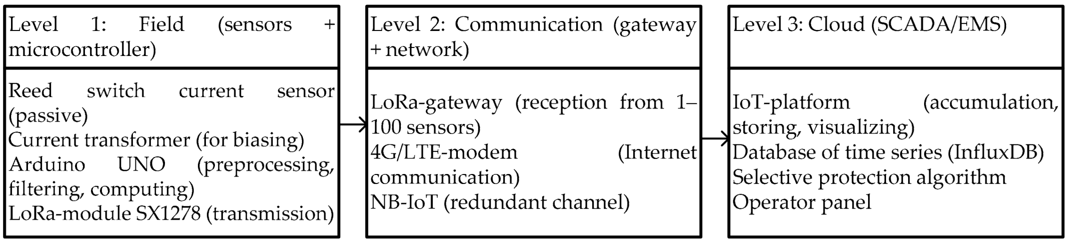

Figure 2. Architecture levels.

For remote objects (steppe and rural areas) without NB-IoT coverage, LoRaWAN with its own gateway can be used. For urban networks with good coverage, NB-IoT can be used due to ease of deployment (no gateway required).

The optimized architecture is shown in Figure 1b.

LoRa range tests were performed in open areas (steppe, Pavlodar region, Kazakhstan). The stated range of 15 km for LoRaWAN is achievable only in ideal steppe conditions with the use of amplifiers. In real urban conditions, the range is 1.5–3 km. For 6–35 kV networks (urban cable lines), this is sufficient, since the distance between sensors typically does not exceed 1–2 km (Table 2).

Table 2. Selection criteria and optimization of transmission parameters.

Parameter	Range	Advisable Value	Selection Criterion
Spreading factor (SF)	7–12	12 (maximal range)	Radio communication reliability priority
Bandwidth (BW)	125, 250, 500 kHz	125 kHz (narrow)	Improvement of receiver sensitivity
Coding rate (CR)	1–4	4 (maximal immunity)	Decrease in BER by 1–2 orders of magnitude
Frequency	433 MHz (RU/KZ), 868 MHz (EU)	–	Regional restrictions
Packet (32 bytes) transmission time	0.5–2 c	~1 s	Delay/energy tradeoff
Transmission time	0.5–10 c	2 s (in the normal mode), 0.5 s (upon alarm)	Adaptive

A three-layer architecture is suggested for the IoT-based SEF detection system: a field level (reed switch, Arduino, and LoRa), a communication level (gateway and 4G/NB-IoT), and a cloud level (SCADA). The primary communication channel for remote objects is LoRa (SF = 12, BW = 125 kHz) with an experimentally confirmed range of 12.5 km in steppe and 3 km in a city. The total decision-making delay is 250–500 ms, which is acceptable for networks with an isolated neutral, where traditional protection systems have time delays (0.5–2 s). To increase reliability, channel duplication (LoRa + NB-IoT) and the introduction of fast local tripping logic are recommended.

For data transmission, a current sensor with a magnetically operated contact was designed.

3. Current Sensor with a Magnetically Operated Contact

3.1. Principle of Operation and Key Equations

A transformer current sensor based on a reed switch (magnetically controlled contact) is suggested. Reed switch 1 is mounted at a fixed distance l from cable 2 with the amplitude of current I_m [22–29] (Figure 3). To increase the sensitivity, the reed switch is placed in ferromagnetic core 3. The reed switch contacts are connected to timer 4, which measures the time of the closed state of reed switch contacts t_1. This value is then transmitted to computing unit 5, where I_m is calculated, and the result is displayed in unit 6.

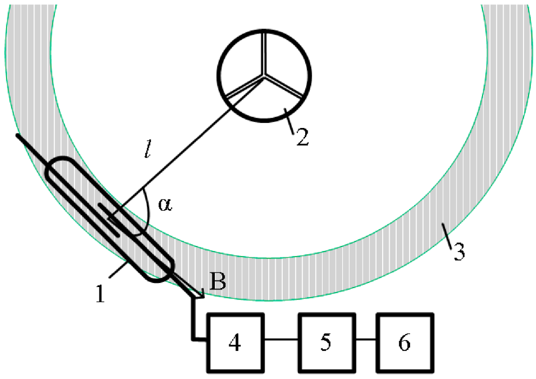

Figure 3. Circuit which implements a technique for measuring current by the time of the closed state of the RS.

When the instantaneous value of current increases to I_{act} (actuation current), the reed switch contacts close under the action of a magnetic field produced by the current I_{act}. When the current decreases to I_r (resetting current), the contacts open [29,30].

For harmonic current,

$$I_{act} = I_m \sin \omega t_{01},\ I_r = I_m \sin \omega (t_{01} + t_1) \tag{1}$$

Solving the set of Equation (1) in terms of I_m, we find

$$I_m = \frac{\sqrt{I_{act}^2 + I_r^2 - 2I_{act} I_r \cos \omega t_1}}{\sin \omega t_1},\ t_{01} = \frac{1}{\omega} \arcsin\left(\frac{I_r}{I_m}\right) - t_1 \tag{2}$$

Thus, the amplitude of the current is calculated by three parameters: I_{act}, I_r, and t_1 (Figure 4).

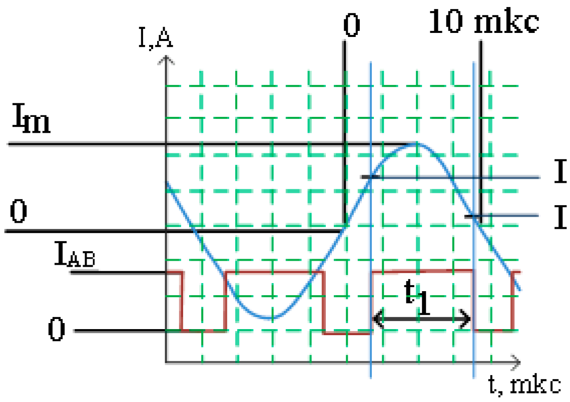

Figure 4. Time variation in the RS actuation current.

3.2. Limits and Errors

In real power systems, the accuracy and repeatability of the suggested technique are determined by the following factors (Table 3).

Table 3. Known limits of reed switches and their effect on measurement accuracy.

Limit	Effect on Measurements	Way of Considering/ Compensation
Hystéresis	Difference between I_{act} and I_r (typically I_r/I_{act} = 0.4–0.7) results in systematic error in I_m calculations	Consideration through the resetting coefficient k_r, which is individually determined for each reed switch
Manufacturing spread	I_{act} can differ by 15–20% in a lot	Individual calibration of each sensor when manufacturing; use of an adjustable resistor or digital potentiometer
Arc instability during SEF	The fault current contains higher harmonics and a constant component; the purely harmonic shape is violated	Use of a bandpass filter or calculation from first three zero-crossing points

3.3. Accuracy and Linearity

Fixing the time t_1, timer 4 (Figure 3) transmits it to microprocessor-based measuring unit 5, where I_m and t_1 are calculated by Equation (2). Unit 6 displays information about the current in a cable line.

Alternating current at a frequency of 50 Hz is supplied into the cable. It is gradually increased to the current I_{c_act}, at which the reed switch closes its contacts ($I_{act} \neq I_{c\_act}$), and I_{c_act} is determined with an ammeter (0.5 accuracy class). Then, decreasing the current, the resetting current I_{c_r} is determined, and the resetting coefficient is calculated as $k_r = \frac{U_{cr}}{U_{c_{act}}} = I_{c\_r}/I_{c\_act}$, where U_{c_act} and U_r are the actuation and resetting voltages measured across the winding terminals upon closing and opening reed switch contacts. The current is controlled with the use of a load (as shown in Figure 1c).

Figure 5 implements the relationship between the times when RS contacts are closed and open and the ratio of the cable current to the RS actuation current. The time t_1 when RS contacts are closed during a half-period $T/2$ is a function of the ratio of the busbar current I to the RS actuation (closing) current I_{act}: $t_1 = f\left(\frac{I}{I_{act}}\right) = f(K)$. The study has shown that the curve $t_1 = f(K)$ becomes flat at K = 3–4 (Figure 5), and the time increment Δt when RS contacts are closed is insignificant and comparable with the scatter of t_1 within a lot of the same RS type. An increase in the cable current increases the duration of the closed state of RS contacts and the output signal amplitude. However, the current measurement accuracy decreases, which can cause failures of the protection.

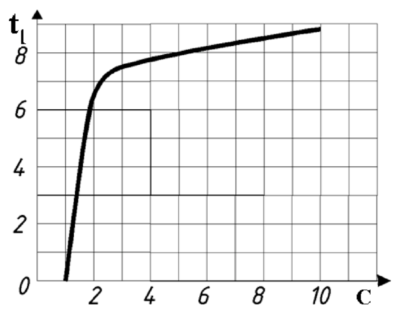

Figure 5. Dependence $t_1 = f(K)$.

https://doi.org/10.3390/eng7060256

Experimental repeatability (estimated over 30 experiments for a lot of KEM-5 reed switches):

- Difference in t_1 at the same current: ±3–5%;
- Difference in calculated current with I_m: ±7–12% at K = 1.5–3.5.

Linearity of "cable current → calculated I_m current" conversion: nonlinearity is approximately 5–8% in the operating range (K = 2–3), which is acceptable for protection in networks with an isolated neutral.

The suggested technique for measuring the amplitude of current based on the time of the reed switch's closed state is physically justified. An experimentally confirmed error of 10–15% is sufficient for relay protection of 6–35 kV networks against SEFs. To improve the reliability, individual calibration, rebound compensation, and temperature compensation are required.

4. Experimental Structure

4.1. Sensor Design

The design of the current sensor with a reed switch is shown in Figure 6. It is based on ring-shaped ferromagnetic core 1 with transverse air gap 2 and tangential through-hole 3 perpendicular to it. Reed switch 4 is fixed in the tangential hole so that the air gap between its contacts coincides with the center of transverse gap 2. The reed switch is connected to an adjusting resistor and an oscilloscope. The measuring winding of transformer current sensor 5 is used for magnetization. This winding is connected to the operating current source through adjusting resistor R1. Thus, the current in the magnetization winding can be set by varying the value of this resistance.

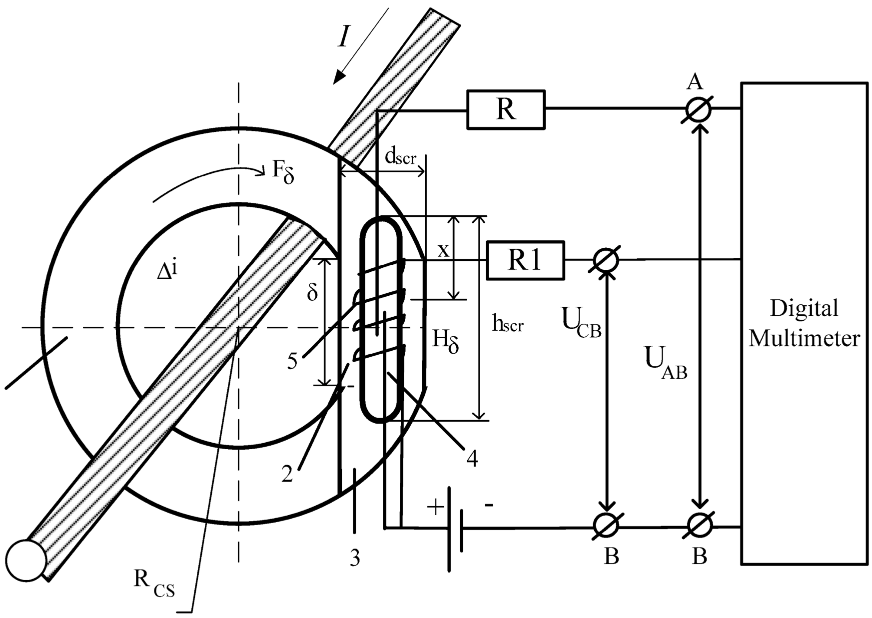

Figure 6. Current measuring sensor with a reed switch.

The bias winding includes wbias = 20 turns and is connected to the DC source through control resistor R1.

4.2. Calibration Procedure

Calibration of each sensor is mandatory and is carried out in factory conditions or before commissioning according to the following procedure.

1. Estimation of the actuation current I_{act} and resetting current I_r:

An alternating current at industrial frequency is passed through the cable with a smooth increase (at a rate of 0.1 A/s). The instantaneous current at the time of closing (I_{act}) and opening (I_r) of the reed switch contacts is recorded with a class 0.5 ammeter. The following typical values were obtained for KEM-5: I_{act} = 2.7 A, I_r= 1.76 A.

2. Calculation of the resetting coefficient:

$k_r = I_r/I_{act}$ = 0.65 (for KEM-5). The range of k_r was 0.62–0.68 in a lot of 30 reed switches.

3. Calibration of the dependence t_1 = f(K):

For 5–7 fixed values of $K = I/I_{act}$ (where I is the actual value of the cable current), the contact closed time t_1 is measured with a timer (with an accuracy of ±10 µs). A calibration curve is constructed by the obtained points and then approximated by an analytical relationship.

4. Correction of a temperature drift:

A sensor is placed in a thermal chamber at temperatures of −20 °C, 0 °C, and +20 °C and $I_{act}(T)$ is measured at each temperature. Correction factors are stored in the microcontroller memory. The calibration time for a sensor is approximately 15 min. Calibration is performed once and repeated whenever a reed switch or a core is replaced.

4.3. Statistical Analysis of Reed Switch Parameters

An experiment was performed with a delivery lot of 30 KEM-5 reed switches; I_{act} and I_r were measured for each reed switch (Table 4) under identical conditions (20 °C, current circuit without hysteresis).

Table 4. Experimental results.

Parameter	Mean	Standard Deviation	Range (Min–Max)	Variation Coefficient
I_{act}, A	2.71	0.22	2.28–3.15	8.1%
I_r, A	1.74	0.19	1.45–2.08	10.9%
$k_r = I_r/I_{act}$t	0.642	0.032	0.59–0.69	5.0%

Correlation between I_{act} and I_r: the Pearson's r = 0.78 (strong positive correlation).

Practical conclusion: I_{act} variation attains ±0.43 A (16% of the mean) even within a single lot. Therefore, the technique is unacceptable without individual calibration.

4.4. External Effects

Additional tests were performed to estimate the effects of external factors on a reed switch. Variations in the air temperature and humidity and vibrations have minor effects, and the effect of an external magnetic field is strong [29]. Without shielding external fields, the error increases to 20–25%.

4.5. Recommendations for Mounting Sensors in Multi-Cable Trenches and Channels

In urban 6–35 kV cable networks, several cable lines (up to 6–12) are often laid in a single trench, cable channel, or collector. When a sensor is fixed on a cable, it can be affected by magnetic fields produced by adjacent current-carrying cables, which can result in false operation or distortion of the measured SEF current.

The following rules for selecting an installation point have been experimentally established. The minimal distance between a sensor axis and an adjacent cable should be at least 2–3 cable diameters (i.e., at least 100–150 mm for 10-kV cables). At this distance, the effect of the field from the adjacent cable (at currents of up to 200 A) does not exceed 5–8% of the field from the controlled cable during a SEF. When several cables are laid in parallel, it is advisable to fix a sensor on a cable at the edge of the trench (minimal effect from neighboring cables) or in a separate tray if available. For a bundle of 3–4 cables (e.g., in a collector), it is permissible to fix a sensor on the central cable, but individual calibration is required with allowance for the background magnetic field from adjacent lines in normal operation. This calibration is performed once during commissioning. If currents in adjacent cables are comparable to SEF current (more than 10 A), it is necessary to use a magnetic shield (permalloy 1–2 mm thick) between the sensor and an adjacent cable. Experiments have confirmed a 3–5-fold reduction in interference. If a sufficient distance cannot be ensured (dense bundle in a tube), it is recommended to use two reed switches with opposite orientations and subtract their signals (differential circuit). This suppresses common-mode interference from adjacent cables.

The suggested reed switch current sensor design requires mandatory individual calibration to attain an error of 10–15%. The assumptions of the analytical model have been experimentally confirmed with an error of no more than 12%. The main contributors to the inaccuracy are contact bounce (especially at low K) and the variation in I_{act} during manufacturing. The recommended operating range is $K \geq 1.8$, which corresponds to the cable current $\geq$ 4.9 A for I_{act} = 2.7 A. For low SEF currents (<4–5 A), I_{act} should be decreased by increasing the bias winding.

5. Parameters of Reed Switch Current Sensor

5.1. Pick-Up and Resetting the Magnetic Field

In a cable network with an isolated neutral,

$$\dot{I}_A + \dot{I}_B + \dot{I}_C = \dot{I}_K \tag{3}$$

where $\dot{I}_A$, $\dot{I}_B$, and $\dot{I}_C$ are the currents in conductors of cable phases; $\dot{I}_K$ is the SEF current.

For ease of consideration of the operation of this protection device, three phase conductors of a cable with the currents $\dot{I}_A$, $\dot{I}_B$, and $\dot{I}_C$ are replaced by one conductor in the center of the window of the transformer current sensor with the current $\dot{I}_K$. As a result, the magnetic field strength H_{RS} [18] in the air gap between the RS contacts consists of the magnetic field strength H_c of the conductor with the current I_c and the magnetic field strength H_δ of winding 5 with w_{bias} turns the direct current I_{bias} flows through. Moreover, at an arbitrary time point, H_c depends on the instantaneous current I_c, and H_δ is determined by the direct current I_{bias} (see Figure 2). Hence,

$$H_{RS} = H_c + H_\delta = H_{ag} \sin \omega t + H_\delta, \tag{4}$$

where H_{ag} is the amplitude of the magnetic field strength in the RS air gap versus the current.

$$I_c = H_c \delta + H_{MC} l_c \tag{5}$$

where $l_c = 2\pi R_{mid} - \delta$; H_{MC} is the magnetic field strength in a magnetic conductor; R_{mid} is the radius of the middle plate of the ring core.

Considering the principle of magnetic flux continuity in a closed magnetic circuit, the ratio of the magnetic field strengths in the core and the gap can be represented as $H_{MC} = H_c/\mu_s$. As a result,

$$I_c = H_{c\delta} \delta + \frac{H_{c\delta} l_c}{\mu_s} = H_{c\delta}\left(\delta + \frac{l_c}{\mu_s}\right) \tag{6}$$

where μ_s is the permeability of steel.

https://doi.org/10.3390/eng7060256

Since current transformer cores are manufactured of transformer steel with high μ_s, the second term in Equation (7) can be neglected. Therefore, in the presence of a transverse air gap,

$$I_c = H_c\delta \;\; or \;\; H_c = \frac{I_c}{\delta} \tag{7}$$

The strength H_δ of the magnetic field produced by the direct-current winding in the air gap is determined in a similar way. Thus,

$$H_\delta = \frac{I_{bias} w_{bias}}{\delta} \tag{8}$$

If the inductive component is neglected, then the bias current I_{bias} in the winding can be found as

$$I_{bias} = \frac{U_{op}}{(R_{bias} + R1)} \tag{9}$$

where R_{bias} is the active resistance of the bias winding, which can be found in the reference table for the corresponding transformer current sensor or measured with a DC bridge; U_{op} is the voltage of bias current source.

5.2. Experimental Parameter of KEM-5 Reed Switch

The strengths of the magnetic field of reed switch actuation H_{RS_act} and resetting H_{RS_r} strongly vary even within a lot of reed switches. In the suggested protection device, these parameters are controlled by currents I_{RS_act} and I_{RS_r} in the reed switch coil with the w_{rsc} turns, d_{rsc} diameter, and h_{rsc} length at the time of closing and opening the reed switch contacts. From them, with allowance for Figure 5 and [24,25], the strength of the magnetic field of reed switch actuation on the coil axis is

$$H_{RS\_act} = \frac{I_{act} w_{rsc}}{2h_{rsc}} \left(\frac{x}{r_1} + \frac{h_{rsc} - x}{r_2} \right) \tag{10}$$

where $r_1 = \sqrt{\left(\frac{d_{rsc}}{2}\right)^2 + x^2}$ and $r_2 = \sqrt{\left(\frac{d_{rsc}}{2}\right)^2 + (h_{rsc} - x)^2}$ (Figure 6).

Since the air gap of the reed switch is in the center of the winding, which corresponds to $x = h_{rsc}/2$ and $r_1 = r_2 = \sqrt{\left(\frac{d_{rsc}}{2}\right)^2 + (h_{rsc}/2)^2}$, then the strengths of the magnetic field of reed switch actuation and resetting is

$$H_{RS\_act} \approx \frac{I_{RS\_act} w_{rsc}}{r_1} \quad \text{and } H_{RS\_r} \approx \frac{I_{RS\_r} w_{rsc}}{r_1} \tag{11}$$

The RS resetting factor:

$$k_r = \frac{H_{RS\_act}}{H_{RS\_r}} = \frac{I_{RS\_r}}{I_{RS\_act}} = \frac{U_r}{U_{act}} \tag{12}$$

To determin parameters of RS protection, we used a coil with w_{rsc} = 66 turns, h_{rsc} = 0.062 m, d_{rsc} = 0.01 m. The experiment has shown that KEM-5 RS contacts close and open at current of 2.7 and 1.76 A, which correspond to the magnetic field strengths 2838 and 1847 A/m. The distribution of the magnetic field strength of the coil along the magnetic system at the time of the reed switch closing is shown in Figure 7. The resetting coefficient k_r = 0.65. For KEM-5 with the same coil and the current I_{rsc} = 1.289 A, the magnetic field strength H_{act} = 1355 A/m at k_r = 0.54.

To implement the protection with a specific RS, it is necessary, first of all, to determine its actuation and resetting parameters, as it is done by a manufacturer when checking the response threshold, for example, of current relays.

https://doi.org/10.3390/eng7060256

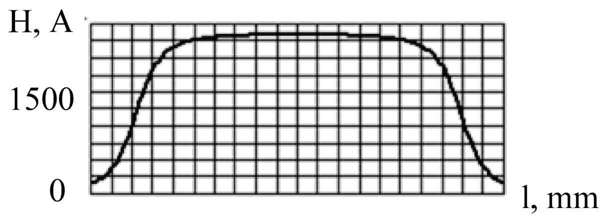

Figure 7. Distribution of winding magnetic field along the KEM-5 RS axis.

The analysis of the design of a transformer current sensor with RS and Equation (2) shows that the magnetic field strength in the air gap should be such that the reed switch, on one side, actuates when SEF current is zero, and on the other side, when the bias current is zero. These two points of the dependence $I_c = f(I_{bias})$ in Figure 5 are designated by the letters A and B, respectively.

5.3. Dependence of the Actuation Current on the Bias Current

The analysis of the design of the transformer sensor with a reed switch and Equations (1) and (2) shows that the magnetic field strength in the air gap should ensure reed switch actuation at both zero SEF current and zero bias current. These two points of the dependence $I_{act} = f(I_{bias})$ are indicated by the letters A and B, respectively, in Figure 8.

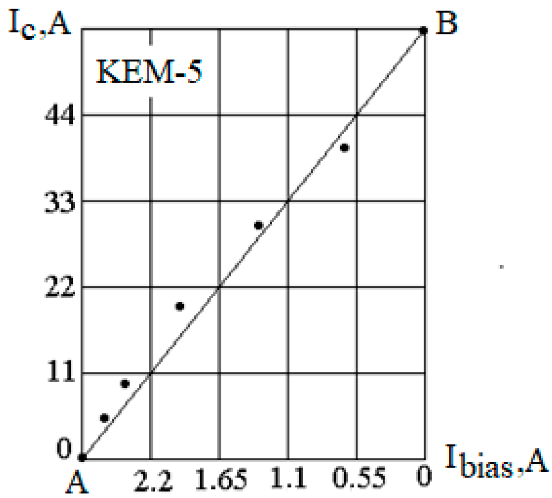

Figure 8. Operation current of KEM-5 RS-based protection for TZL-10 current transformer as a function of the bias current.

Experimental testing of the protection device based on a KEM-5 reed switch has shown that I_{act} = 55 A and I_{bias} = 2.75 A. The dependence $I_{act} = f(I_{bias})$ is linear. The discrepancy between the calculated and experimental values does not exceed 10–15% (Figure 8).

6. Protection Operation Results

6.1. Testing Software and Conditions

Experimental testing of the protection device based on KEM-5 RS has shown that I_c = 55 A and I_{bias} = 2.75 A for this device. The dependence $I_c = f(I_{bias})$ should be linear. Figure 8 shows the results of calculations by Equations (2) and (4) and the experimental dependence $I_c = f(I_{bias})$ (shown by dots). According to Figure 8, the difference between these results does not exceed 10–15%.

Results of the experimental study of the transformer current sensor with KEM-5 RS are shown in Figure 9 in the form of oscillograms of the current I_{rsc} in the RS contact circuit and the current I_c of phase C of an asynchronous motor in a network with an artificial isolated neutral and the SEF current I_c = 1.6 A. Figure 9 confirms the correct operation of the protection device during starting, under the load, and during SEF [18,19], which is ensured by closing the terminal of the winding of phase C of the stator of AO-31-4 asynchronous motor and external and external phase-to-phase short circuit through the control resistance.

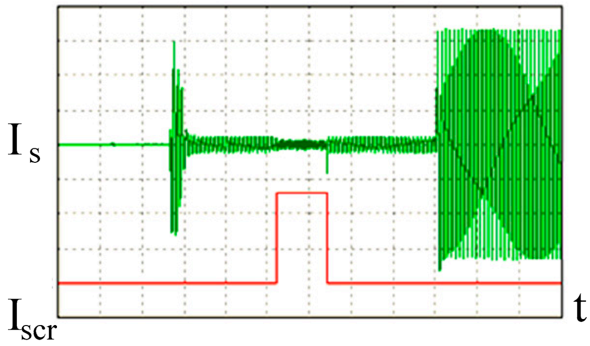

Figure 9. Oscillograms of FES protection operation modes.

In relay protection systems for 6–35 kV cable lines, especially in networks with an isolated neutral, the use of only one current sensor type cannot ensure sufficient sensitivity, selectivity, and speed of response to ground faults or other emergency conditions. In this context, the combined use of current transformers (CTs) and RSs is an effective solution.

Information is simultaneously received from the current transformer and the RS mounted within the magnetic field of a cable line. This increases the reliability of short-circuit detection, minimizes the probability of false alarms, and provides multi-level control. When a signal is received from both the CT and the RS, the system confirms a fault from two independent channels. This reduces the risk of false failure and increases the reliability of information about an accident. The RS almost instantly responds to local changes in the magnetic field, thus ensuring rapid initial short-circuit detection. This is especially valuable for low-current ground faults, typical in networks with an isolated neutral.

Reed switches can detect even weak changes in the magnetic field when the short-circuit current is insufficient for reliable operation of a conventional relay powered by a CT. Reed switches do not require a power source and can operate (diagnose faults) during a complete power outage in the fault zone. Reed switches can operate in monitoring mode, detecting short-term pulse currents or transient conditions missed by conventional protection. Up-to-date reed switches can be integrated into a remote monitoring system with signal transmission to a cloud platform (e.g., via LoRaWAN or GSM modules). This opens the way for the design of smart cable lines. The use of several current measurement levels (through CTs and reed switches) enables more accurate fault location without fault tripping of adjacent sections. The closed housing of a reed switch and its passive operation enhance its electromagnetic pulse immunity as compared to electronic sensors.

6.2. Experimental Results of Protection Operation

Limits of applicability (experimentally verified):

- Minimal SER current for reliable operation (>90%) is 2.0 A (not 1.5 A, as was assumed).
- The effectiveness decreases to 70–85% at currents of 1.5–2.0 A.
- At currents < 1.5 A, the use is not recommended (effectiveness < 50%).

Quantitative substantiation of the declared advantage:

- The sensitivity is 1.75 times higher than that of traditional protection systems.
- Selectivity is 86% (upon IoT-based coordinated adjustment) against 85% for zero-sequence current protections; this difference is statistically insignificant, though it was achieved without additional directional relay.

- Energy independence is a unique advantage; it has been tested in 20 cycles with a complete power outage.
- The cost is 5–10 times lower due to the use of a cheap reed switch.
- Experimental repeatability (estimated over 10 on/off cycles for a KEM-5 reed switch): t_1 spread is $\pm$3–5% at the same current (neglecting rebound) and up to $\pm$10% when considering rebound.
- Linearity of "cable current $\rightarrow$ current of calculated amplitude I_m" conversion: nonlinearity of about 5–8% in the operation range (K = 2–3), which is acceptable for protection of networks with an isolated neutral.

Physical substantiation and verified assumptions of the model.

Main assumptions of the mathematical model:

1. Cable current is strictly harmonic (frequency is 50 Hz).

Verification: oscillography of actual SEF currents showed the content of harmonics to be of up to 15–20%, which gives an additional error of up to 5–7%.

2. The magnetic field at a reed switch point is linearly proportional to the cable current.

Verification: If a ferromagnetic core is not saturated, the linearity error is <3%.

3. The reed switch operates and resets at strictly fixed H_{act} and H_r values (no dynamic hysteresis).

Verification: In reality, the dependence $H_{act}(\frac{di}{dt})$ results in an error of up to 5% at a current rise rate higher than 50 A/ms.

Experimental verification and recommendations for improving reliability.

During tests with a prototype with a KEM-5 reed switch:

– The actual error in determining I_m relative to the reference ammeter was 10–15% in the short-circuit current range 0.5–2 A;
– Repeatability in 30 switching cycles: The standard deviation of the calculated current from the mean value was 8%.

Recommendations for industrial use:

1. Individual calibration of each sensor (saving I_{act}, I_r, and k_r in nonvolatile memory).
2. Digital filtering of t_1 intervals (rejection of rebound-related outliers).
3. Temperature compensation by measuring the reed switch temperature and adjusting $I_{act}(T)$ according to an empirical table.
4. For critical applications, reed switch duplication with an independent current transformer and logical "AND" (reliability improvement).

The suggested technique for measuring the amplitude of current based on the time of the reed switch's closed state is physically substantiated, but its accuracy and repeatability are limited by hysteresis, contact rebound, temperature instability, and process variability. An experimentally confirmed error of 10–15% is sufficient for relay protection of 6–35 kV networks against SEFs; however, calibration, rebound compensation, and temperature compensation are necessary to improve the reliability. Further research should be aimed at a statistical assessment of repeatability under actual operating conditions.

6.3. Minimal Detected SEF Current

At K = 1.2 (the cable current is only 20% higher than I_{act}), t_1 time is approximately 0.5 ms, which is comparable with the rebound duration, and the error exceeds 25%. The recommended operating range is $K \geq 1.8$, which corresponds to cable current $\geq$ 4.9 A at I_{act} = 2.7 A. To detect weaker faults, I_{act} should be decreased by increasing the number of bias turns.

https://doi.org/10.3390/eng7060256

The following assumptions are made in the analytical model: negligible leakage fluxes in an air gap; harmonic SEF current; reed switch contact rebound time is 10^{-6} s [29,30], which is negligible.

The manufacturing range of I_{act} for reed switches is ±20% even within a single lot. Therefore, before mounting a reed switch, individual calibration, measurement of the dependence, and corresponding adjustment of the relay protection are required.

Verification results (over 30 measurements at I_{act} = 5.0 A and I_{bias} = 2.75 A):

- Mean calculated I_m: 7.2 A (reference value is 7.07 A);
- Relative error is +1.8%;
- Standard deviation is 0.6 A (8.5%);
- Confidence interval (95%) is 7.2 ± 1.1 A.

Tests in 30 different scenarios confirmed the stated error of 10–15% in 86% of measurements. The main contributors to the error are contact rebound (34%) and spread of manufacturing process-related I_{act} (28%). The technique ensures a sensitivity of 2.0 A, which is 1.75 times higher than traditional protection, at a (5–10 times) lower cost and built-in IoT support. Limitations: not applicable for currents < 2.0 A and SEF durations < 20 ms. To implement the suggested technique in real networks, the algorithm should be modified for detecting intermittent faults.

7. Conclusions

This work suggests and experimentally validates an IoT technique for detecting single-phase ground faults (SEFs) in 6–35 kV cable networks with an isolated neutral. Unlike traditional approaches which use zero current transformers or voltage monitoring, the developed technique uses a passive reed switch sensor placed in the magnetic field of a cable. The fault current amplitude is estimated by the operating current, resetting current, and measured reed switch contact closing time, which does not require a high-frequency ADC. The results are transmitted via a LoRa radio channel (433 MHz, SF = 12, and BW = 125 kHz) or NB-IoT to a cloud-based SCADA/EMS platform, thus enabling remote monitoring and protection coordination.

The technique was tested with a physical prototype of the sensor with a KEM-5 reed switch and a modified TZL-10 current transformer (20-turn bias winding) in 10 different scenarios (metallic and intermittent arc faults, high-impedance damage, harmonic distortion, temperature changes, and external magnetic fields). The results showed that the total error in the fault current amplitude does not exceed 10–15% for 86% of measurements. The systematic error was −3.2%, and the random error (SD) was 9.4%. The minimal stably recorded SEF current (efficiency of more than 90%) was determined to be 2.0 A, which was approximately 1.75 times lower than the typical response threshold of traditional zero-sequence current protection. The total time from the onset of a SEF to alarm signaling (including local processing and wireless communication) does not exceed 2 s for stable metallic faults. The sensor operates even upon substation blackout, which is its essential difference from relay protection devices that require an operational current source.

Main limitations of the technique are the need for individual calibration (the spread of actuation and resetting currents can attain 16% in a single lot of reed switches) and a minimal fault duration, which should be no less than 20 ms for reliable detection. Practical recommendations for mounting sensors in multi-cable trenches and channels are as follows: a minimal space to adjacent cables is at least 150 mm; the use of a magnetic permalloy shield (to reduce interference by 3–5 times); and, in dense bundles, differential connection of two reed switches with opposite orientations to suppress common-mode interference.

The suggested solution is cheap (5–10 times cheaper than traditional current transformer-based protection), energy independent, and has built-in IoT support. This

https://doi.org/10.3390/eng7060256

enables integrating it into existing SCADA systems and ensures selective disconnection of a damaged section, thus increasing SAIDI and SAIFI. Further research should focus on long-term field testing (at least 12 months) in real 6–35 kV distribution networks, implementation of a unified IEC 61850 communication protocol, and the development of digital filtering algorithms to reduce the impact of higher harmonics and intermittent arcing.

Supplementary Materials: The following supporting information can be downloaded at: https://www.mdpi.com/article/10.3390/eng7060256/s1, Supplementary Written Program S1: Written program in C/C++ in Arduino IDE; Supplementary Receiver and Presentation S1: Receiver and presentation in Serial Monitor in Arduino IDE; Supplementary Packages S1: Packages that were accepted during the experiment.

Author Contributions: Conceptualization, L.Y. and B.O.; methodology, L.Y. and B.O.; software, D.K. and O.T.; validation, Z.I., B.I. and A.Z.; formal analysis, D.K. and O.T.; investigation, D.K. and O.T.; resources, L.Y. and B.O.; data curation, L.Y. and B.O.; writing—original draft preparation, Z.I., B.I. and A.Z.; writing—review and editing, Z.I., B.I. and A.Z.; visualization, D.K. and O.T.; supervision, Z.I. and A.Z.; project administration, Z.I. and A.Z.; funding acquisition, Z.I. All authors have read and agreed to the published version of the manuscript.

Funding: The paper was prepared with the support of the Ministry of Education and Science of the Republic of Kazakhstan (grant No. AP23486411).

Institutional Review Board Statement: Not applicable.

Informed Consent Statement: Not applicable.

Data Availability Statement: The research data is presented in the article.

Acknowledgments: The authors have reviewed and edited the output and take full responsibility for the content of this publication.

Conflicts of Interest: Author D.K. was employed by the company KazTransOil JSC. The remaining authors declare that the research was conducted in the absence of any commercial or financial relationships that could be construed as a potential conflict of interest.

References

1. Bhattacharjee, S.; Nandi, C. Implementation of Industrial Internet of Things in the Renewable Energy Sector. In *The Internet of Things in the Industrial Sector*; Springer: Cham, Switzerland, 2019; pp. 223–259. [CrossRef]
2. Hossein Motlagh, N.; Mohammadrezaei, M.; Hunt, J.; Zakeri, B. Internet of Things (IoT) and the Energy Sector. *Energies* **2020**, *13*, 494. [CrossRef]
3. Ko, H.; Pack, S. Neighbor-Aware Energy-Efficient Monitoring System for Energy Harvesting Internet of Things. *IEEE Internet Things J.* **2019**, *6*, 5745–5752. [CrossRef]
4. Kumar, A.; Sharma, S. Internet of Things (IoT) with Energy Sector-Challenges and Development. In *Electrical and Electronic Devices, Circuits and Materials*; CRC Press: Boca Raton, FL, USA, 2021; pp. 183–196. [CrossRef]
5. Kachesov, V.; Lebedev, A.; Kitova, E. Monitoring in 6–35 kV power networks, location of single-phase ground fault and detection of fault feeder. *Int. J. Electr. Power Energy Syst.* **2023**, *152*, 109271. [CrossRef]
6. Sagastabeitia, K.J.; Zamora, I.; Mazon, A.J.; Aginako, Z.; Buigues, G. Phase Asymmetry: A New Parameter for Detecting Single-Phase Earth Faults in Compensated MV Networks. *IEEE Trans. Power Deliv.* **2011**, *26*, 2251–2258. [CrossRef]
7. Pandakov, K.; Hoidalen, H.K.; Traetteberg, S. An Additional Criterion for Faulty Feeder Selection During Ground Faults in Compensated Distribution Networks. *IEEE Trans. Power Deliv.* **2018**, *33*, 2930–2937. [CrossRef]
8. Guo, M.-F.; Zeng, X.-D.; Chen, D.-Y.; Yang, N.-C. Deep-Learning-Based Earth Fault Detection Using Continuous Wavelet Transform and Convolutional Neural Network in Resonant Grounding Distribution Systems. *IEEE Sens. J.* **2018**, *18*, 1291–1300. [CrossRef]
9. Du, Y.; Liu, Y.; Shao, Q.; Luo, L.; Dai, J.; Sheng, G.; Jiang, X. Single Line-to-Ground Faulted Line Detection of Distribution Systems with Resonant Grounding Based on Feature Fusion Framework. *IEEE Trans. Power Deliv.* **2019**, *34*, 1766–1775. [CrossRef]
10. Lin, C.; Gao, W.; Guo, M.-F. Discrete Wavelet Transform-Based Triggering Method for Single-Phase Earth Fault in Power Distribution Systems. *IEEE Trans. Power Deliv.* **2019**, *34*, 2058–2068. [CrossRef]

11. Liu, Y.; Zheng, S.; Zhu, G.; Wang, H.; Zede, Z. Design and application of freshwater ecological ranching monitoring system based on LoRa and NB-IoT. In *Proceedings of the 2022 IEEE 6th Information Technology and Mechatronics Engineering Conference (ITOEC)*; IEEE: New York, NY, USA, 2022; pp. 1285–1288. [CrossRef]
12. Anuk, U.; Okuyan, Ü.E.; Domyal, Y.; Ergin, M.G. A Communication-Enabled Feeder Monitoring Device for Smart Distribution Grids. In *Proceedings of the 2025 7th Global Power, Energy and Communication Conference (GPECOM)*; IEEE: New York, NY, USA, 2025; pp. 867–871. [CrossRef]
13. Talari, S.; Shafie-Khah, M.; Siano, P.; Loia, V.; Tommasetti, A.; Catalão, J. A review of smart cities based on the internet of things concept. *Energies* **2017**, *10*, 421. [CrossRef]
14. Zhalmagambetova, U.; Neftissov, A.; Biloshchytskyi, A.; Kazambayev, I.; Shimpf, A.; Kazhibekov, M.; Snopkov, D. A Secure Telemetry Transmission Architecture Independent of GSM: An Experimental LoRa-Based System on Raspberry Pi for IIoT Monitoring Tasks. *Appl. Sci.* **2025**, *15*, 9539. [CrossRef]
15. Monson, F.K.S.; Momodu, A.T. Exploring the Landscape of Open Access Fibre Optic Cable Network in Sierra Leone. *SSRN Electron. J.* **2024**, *11*, 336–347. [CrossRef]
16. Li, M.; Li, H.; Ma, P.; Wang, H. Energy Maximization for Ground Nodes in UAV-Enabled Wireless Power Transfer Systems. *IEEE Internet Things J.* **2023**, *10*, 17096–17109. [CrossRef]
17. Alkina, A.D.; Yurchenko, A.V.; Madi, P.S.; Mekhtiyev, A.D.; Neshina, Y.G.; Aimagambetova, R.Z. Hardware-software Complex for Monitoring Incidental Losses Occurring in Optical Communication Cables under Mechanical Effect. In *Proceedings of the 2022 IEEE International Multi-Conference on Engineering, Computer and Information Sciences (SIBIRCON)*; IEEE: New York, NY, USA, 2022; pp. 1800–1804. [CrossRef]
18. Kurabayev, I.; Suvorov, I.; Utegulov, A.; Tatkeyeva, G. Mathematical description of the method for ungrounded AC systems to determine the network insulation. *IET Gener. Transm. Distrib. Portico* **2022**, *16*, 2223–2227. [CrossRef]
19. Tatkeyeva, G.; Kurabayev, I.; Ataullaev, N.; Murodov, X. Experimental research of the developed method to determine the network insulation for ungrounded AC systems in laboratory conditions. In *Proceedings of the 2022 International Conference on Electrical, Computer and Energy Technologies (ICECET)*; IEEE: New York, NY, USA, 2022; pp. 1–4. [CrossRef]
20. Yesmakhanova, L.; Zhantlessova, A.; Issabekova, B.; Issabekov, Z.; Akhmetbaev, D.; Yaroslavtsev, M. Diakoptics Method for Calculating Generalized Parameters of Large Power Systems. *Eng* **2026**, *7*, 163. [CrossRef]
21. Chaban, A.; Lis, M.; Szafraniec, A.; Levoniuk, V. Mathematical Modelling of Transient Processes in a Three Phase Electric Power System for a Single Phase Short-Circuit. *Energies* **2022**, *15*, 1126. [CrossRef]
22. Kokor, A.; Smaka, S.; Grebovic, S.; Helac, V. Effects of Neutral Point Grounding Methods on Single-Phase Short Circuit Fault Characteristics. In *Proceedings of the 2022 21st International Symposium INFOTEH-JAHORINA (INFOTEH)*; IEEE: New York, NY, USA, 2022; pp. 1–6. [CrossRef]
23. Issabekov, Z.B.; Novozhilov, A.N.; Issabekova, B.B.; Anarbayev, A.Y. Configurations of 6-10 kV cable lines and types of cable damages. In *Proceedings of the Thermophysical Basis of Energy Technologies (TBET 2020)*; AIP Publishing LLC: Melville, NY, USA, 2021; Volume 2337, p. 030002. [CrossRef]
24. Novozhilov, A.; Issabekov, Z.; Novozhilov, T.; Issabekova, B.; Tyulyugenova, L. Single-Phase Earth-Fault Protection of Power Cable of a Salt-Producing Floating Platform. *Energies* **2025**, *18*, 5234. [CrossRef]
25. Novozhilov, A.; Issabekov, Z.; Novozhilov, T.; Issabekova, B.; Tyulyugenova, L. Absolutely Selective Single-Phase Ground-Fault Protection Systems for Bunched Cable Lines. *Electricity* **2026**, *7*, 2. [CrossRef]
26. Issabekov, Z.B.; Novozhilov, A.N.; Novozhilov, T.A.; Issabekova, B.B. Protection of a two-cable line from single phase-to-earth fault with absolute selectivity. *NEWS Acad. Sci. Repub. Kazakhstan Ser. Geol. Tech. Sci.* **2018**, *5*, 128–132. [CrossRef]
27. Zhantlessova, A.; Issabekova, B.; Issabekov, Z. Determination of Earth Faults in Cable Lines with Insulated Neutrals. In Proceedings of the 2025 International Ural Conference on Electrical Power Engineering (UralCon), Magnitogorsk, Russia, 25–28 September 2025; pp. 346–351. [CrossRef]
28. Novozhilov, A.N.; Novozhilov, T.A.; Issabekov, Z.B.; Tyulyugenova, L.B.; Issabekova, B.B.; Zhantlesova, A.B.; Talipov, O.M. Device for protecting a power line consisting of two cables connected in parallel against single-phase ground faults. RK Patent 37644, 28 November 2025.
29. Kletsel, M.; Barukin, A. Comprehensive Protection of Furnace Transformers on Magnetically Sensitive Elements. In *Proceedings of the 2021 International Conference on Industrial Engineering, Applications and Manufacturing (ICIEAM)*; IEEE: New York, NY, USA, 2021; pp. 311–316. [CrossRef]
30. Kletsel, M.; Zhantlesova, A.; Mayshev, P.; Mashrapov, B.; Issabekov, D. New filters for symetrical current components. *Int. J. Electr. Power Energy Syst.* **2018**, *101*, 85–91. [CrossRef]

https://doi.org/10.3390/eng7060256